Crystalline ribosomes are present in brains from senile humans

(neurodegeneration/spatial filtering/Hirano bodies/aging/endoplasmic reticulum)

LAURA O'BRIEN*, KIRK SHELLEY*, JAVAD TOWFIGHI†, AND ALEXANDER MCPHERSON*‡

Departments of *Biochemistry and †Pathology, The Milton S. Hershey Medical Center, The Pennsylvania State University,
Hershey, Pennsylvania 17033

ABSTRACT   Paracrystalline inclusions known as Hirano
bodies characteristically appear in the hippocampal region of
the brains of humans exhibiting senile and presenile dementias
as well as several other neurodegenerative diseases. We present
evidence that the currently accepted model for those structures
based on alternating filament sheets is not correct, but that
Hirano bodies are stacked sheets of membrane-bound ribosomal
particles derived from partially degraded rough endoplasmic
reticulum or Nissl substance. Using fluorescence staining with
acridine orange and ethidium bromide, we have shown that the
bodies contain RNA. Spatial filtering of electron micrographs
by Fourier techniques shows that the individual particles that
make up the arrays have a characteristic shape previously re-
ported for the large subunit of eukaryotic ribosomes. The storage
of these ribosomal particles in inclusion bodies may indicate
a quiescent state of protein synthesis in the cells. This with-
drawal of synthetic mechanisms in the hippocampus may have
significant consequences in the loss of ability to consolidate
short-term to long-term memory.

Paracrystalline inclusion bodies (see Fig. 1) known as Hirano
bodies have been found in the brains of humans under various
pathological conditions; they also occur in normal individuals.
They become especially prevalent with advancing age and are
a particularly pronounced histological feature in patients with
senile and presenile dementia caused by, e.g., Pick's disease and
Alzheimer's disease. Although found predominantly in the
pyramidal layer of the hippocampus, they have also been noted
in other neurological tissues under conditions of general de-
generation. In the initial reports, the observations of Hirano
bodies were confined exclusively to the central nervous system.
They were confirmed in patients with amyotrophic lateral
sclerosis and parkinsonism-dementia (1), in a patient with motor
neuron disease (2), in kuru-infected human cerebellum (3), in
mice infected experimentally with scrapie (4), and in an ado-
lescent with hepatocerebral degeneration (5). Hirano bodies
have also been demonstrated in the peripheral nervous system
in a line of mutant hamsters with hind-leg paralysis (6) and in
a retroperitoneal ganglioneuroblastoma from a 4-year-old child
(7). It has also been suggested that they are a nonspecific ac-
companiment to some types of neuronal degeneration and not
necessarily associated with any specific disease (7–9).

Hirano bodies, when sectioned and examined by electron
microscopy, exhibit an interior composed of an ordered lattice
work of alternating lines and electron-dense particles demon-
strating a high degree of periodicity in three dimensions. The
paracrystalline inclusions are spindle shaped and approximately
10 μm long, with a diameter of roughly half that. The indi-
vidual elements that produce the latticework arrangement
appear to be long distinctive fibers or strands with an associated

sequential set of particles occurring at specific intervals. Some
details of this network are shown in Fig. 2.

The structural model proposed to explain the electron mi-
croscopic images yielded by the Hirano bodies is that the
paracrystalline array arises from sheets of filaments with the
fibers of each alternating sheet running perpendicular to those
of adjacent sheets. Thus, the continuous strands represent the
filaments seen longitudinally whereas the electron-dense par-
ticles are presumably the fibers seen in cross section. Detailed
descriptions of this model can be found in refs. 8 and 10. We
contend that this model is incorrect and does not adequately
explain the observations.

If the inclusion bodies were composed of stacks of fibrous
sheets, then every sheet should be essentially independent of
those above and below. In fact, a continuous strand, presumed
to be a filament viewed longitudinally, is seldom if ever ob-
served without the direct association of discrete electron-dense
particles. Virtually all micrographs suggest that every contin-
uous line has directly attached to it a sequential set of the dis-
crete particles in a specific periodic manner. Furthermore, one
would expect the filaments lying in the substrate plane to stain
in a manner at least similar to the filaments seen in cross section,
but they do not. The filaments seen in longitudinal section
should have a diameter the same as those seen in cross section
(i.e., the electron-dense particles); they do not.

If the structure resulted from stacks of fibrous sheets such that
those above and below any individual sheet are identical though
oriented perpendicular to the one between, then there should
never be any preferred pairing between doublets. That is, every
presumed longitudinal filament should be expected to have
electron-dense particles on either side or on both sides simul-
taneously. This, once again, is not observed. Instead we note that
in micrographs of Hirano bodies, the electron-dense particles
never appear simultaneously on both sides of the strands, but
are all oriented only on one side of the strands throughout the
entire inclusion body (i.e., there is a highly polar distribution
of the particles attached to the strands).

To our knowledge there have not been published any mi-
crographs of sections parallel with the planes of the presumptive
sheets that substantiate the proposal of alternating perpendic-
ular fiber arrays nor have any oblique sections appeared that
would serve as well. In normal neuronal cells impregnated with
silver, neurofilaments show argentophilia (11); Hirano bodies
do not (8, 12).

We believe that Hirano bodies are ordered, crystalline arrays
of membrane-bound ribosomes probably originating from
fragmented rough endoplasmic reticulum or Nissl substance.
Further, we propose that these ribosomal arrays probably
represent an inactive, or storage, form for the ribosomes that
arises during periods or stages of dormancy or degeneration.

---

‡ From whom reprints should be requested at: Department of Bio-
chemistry, University of California, Riverside, CA 92521.

Medical Sciences: O'Brien *et al.*

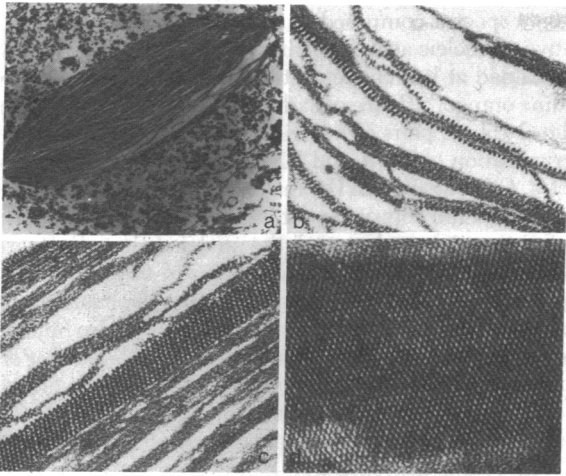*Proc. Natl. Acad. Sci. USA 77 (1980)* 2261

FIG. 1. (a) Electron micrograph showing a typical example of a uranyl acetate- and lead citrate-stained Hirano body in the neuron of a patient with Pick's disease. [Reprinted from Towfighi, J. (1972) *Acta Neuropathol.* 21, 224–231 by permission of the publisher.] (×5400.) (b) A single strand with its electron-dense particles attached at periodic intervals of about 21.5 nm. These strands appear to be the fundamental units of the paracrystalline array. (×45,000.) (c) A series of these strands are seen packed closely together to produce the three-dimensional array. (×56,500.) (d) A view perpendicular to a sheet which constitutes the true fundamental element of the paracrystalline array. One can easily see the distribution of ribosomal particles over the surface of the membrane sheet. (×44,400.)

MATERIALS AND METHODS

Hippocampal tissue obtained from a patient with Alzheimer's disease at autopsy was fixed in formalin and embedded in paraffin by conventional procedures. Five-micrometer sections were stained with hematoxylin and eosin, phosphotungstic acid hematoxylin, colloidal iron, and alcian blue at pH 1.5 and acridine orange (0.001%) at pH 3.8 (11). Ethidium bromide staining was carried out within the same range of variables as used for demonstration of nucleic acids in purified preparations (13), but modified for tissue sections as follows. Sections were treated for 5 min with 1% acetic acid and rinsed in McIllvins's buffer at pH 4.0. The staining solution contained 5 μg of dye per ml of buffer in the presence of 0.1 M NaCl. Sections were treated with the dye solution for 5 min, rinsed thoroughly in buffer, and mounted in Permount.

Concomitant phase-contrast and fluorescence microscopy was used to identify and spectrally analyze the Hirano bodies with an epillumination microspectrophotometer (Leitz Ortholux MPVI). The microscope was equipped with a Xenon light source (XBO-150), a prism monochromator, Ploem illuminator containing a dichroic mirror, Barrier filter (TK495), and a Leitz objective (PV f1 70×, n.,a. 1.15). The emitted light was passed through a circular graded interference filter (Barr–Stroud CGS1/022) into a broad-spectrum photomultiplier (RCA C310934). The excitation wavelength and emission spectra were set and continuously monitored by a photomultiplier system interfaced directly to a PDP 8/I minicomputer. This allowed direct measurement and operator display of emission wavelength.

The spectral profile of each optical element was calibrated such that experimental measurements could be converted to absolute spectra within ±0.5 nm for the excitation monochromator and ±0.7 nm for the measuring monochromator (14). The excitative wavelengths for acridine orange and ethidium bromide were 463 and 460 nm, respectively.

For electron microscopy, formalin-fixed specimens of tissue dissected from Sommer's sector of the right Ammons' horn was

postfixed in Dalton's solution and embedded in araldite. The patient was described at autopsy as an early and asymptomatic case of Pick's disease in conjunction with the presence of rod-shaped neuronal hyalin inclusions (Hirano bodies) and granulovacuolar degeneration of large neurons. Ultrathin sections were photographed under an RCA EMU-4 electron microscope after staining with either uranyl acetate (2% in 50% EtOH) for 45 min or lead citrate (0.4% in 0.1 M NaOH) for 2.5 min. Tilt-stage photographs of stained sections ±24° about both vertical and horizontal axes were also recorded of appropriate sections on a Phillips 400 electron microscope.

For spatial filtering of electron micrographs after visual examination the following procedures were used. An optical diffraction pattern using a 3-m optical bench patterned after that of Klug and Berger (15) with a helium/neon laser light source was recorded on Ortholith transparent film in order to evaluate the level of resolution, the rough orientation of the crystal lattice, and the degree of defocusing (16). Images recorded on glass plates were transferred to Panchromatic film with care to preserve to the greatest degree possible the same relative contrast levels in the micrograph. The Optronics P-1000 microdensitometer used in these studies had a resolution of 50 μm and appropriate magnifications were used to avoid "aliasing effects" (17).

The precise film area to be scanned was determined by a high-speed, low-resolution pass with a raster setting of 200 μm made over the entire micrograph, and the cathode ray tube terminal cursor was used to mark boundary points. This area was statistically analyzed (18) to ensure that the populations of optical densities were well represented and not limited by the scanners' optical density range. Film elements (256 by 256) from the chosen film area were digitized and the data field was circularly shifted by half of the field dimension to ensure that the image origin was at the center of the data set in a process termed "pre-scrambling" (19). The Fourier transform was calculated as a series of one-dimensional fast Fourier transforms along the x axis. The sample was rotated by 90° and a second series of one-dimensional fast Fourier transforms was computed along the new x axis. Although this method (20) requires more time because of the greater number of disk I/O operations than are necessary with totally memory-bound calculations, by this means the size of the largest permissible data set is substantially increased and enables calculation of the transform of a 512 by 512 point array. The low- and medium-resolution peak coordinates were visually approximated, indexed, and marked with the cursor on the cathode ray tube terminal. From these crude positions, peak-locating routines were invoked to refine the positions of the maxima and generate coordinates for high-resolution reciprocal lattice points and those falling between
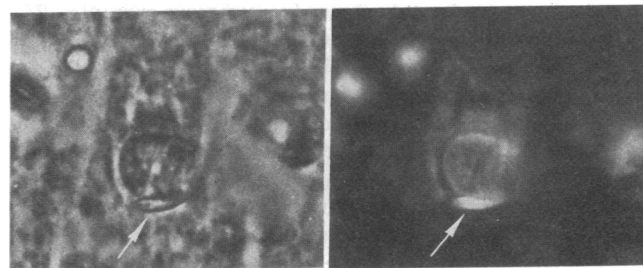

FIG. 2. (*Left*) Phase-contrast photomicrograph showing a Hirano body (arrow) next to a cell nucleus. (*Right*) The identical section stained with acridine orange and viewed under fluorescence conditions. When observed in color, the Hirano body produces a red fluorescence characteristic of RNA–acridine orange complexes whereas the nucleus fluoresces yellow-green as expected for DNA–acridine orange complexes. (×8300.)

initial input peaks. The best possible lattice to fit all observed maxima in the transform was determined by a linear least-squares procedure.

The film was measured with a densitometer at twice the resolution to produce a field of 512 by 512 points. To ensure that an integral number of unit cells were present, a truncation and bilinear expansion was performed (21) by use of the refined cell parameters to detect the fractional unit cells. This was done to ensure that the peak of a diffraction maximum fell precisely on a computational array point. A Fourier transform was then performed with the algorithm of Tukey and Cooley (22) as described above, but calculated only in areas centered on predicted lattice positions. The peak-searching routine was once more applied at each of the predicted lattice positions and used to further refine cell parameters. Each maximum was examined and accepted as a structure factor if it passed certain statistical criteria, including the number of standard deviations by which the peak exceeded the background level. The contrast transfer function of each electron micrograph (16) was determined from the background in the calculated and optical diffraction pattern and was used to correct both the amplitudes and phases of the structure factors, although in most cases the micrographs were recorded close to focus.

The spatially filtered image was calculated again by the fast Fourier transform algorithm. The extent of improvement of final image over original is estimated as the square root of the number of unit cells included in the transform (23). In this study, an approximately 25-fold improvement in the signal-to-noise ratio was realized.

The instrument configuration used in the procedures described above was a PDP 11/40 computer extended to 128 words of core running under the RSX11-M (version III) operating system. The system had one RK05-F disk drive and three RK05-J drives. The peripheral devices available were a line printer, a Tektronics 4010 graphics terminal, a magnetic tape drive, and a Calcomp 365 drum plotter. The central processing time for the 512 by 512 transform was about 15 min.

RESULTS

Electron Microscopy. In our own electron micrographs and those of others we found, with high frequency, single long lines or strands having electron-dense particles attached at periodic intervals (Fig. 1*b*). The average center-to-center period of the beads is approximately 21.5 nm and the beads have diameters of roughly 13.5 nm. Assuming no more than expected shrinkage upon dehydration and fixation, these dimensions are consistent with those of eukaryotic ribosomal particles (24). The individual strands with the attached particles strongly resemble the distribution of particles bound to the membrane surfaces of rough endoplasmic reticulum. As shown by numerous examples (25, 26), they have about the same diameter, periodic distribution, length of period (20 nm), and size ratio of particle to strand.

Histology. From our experiments and those published (27), we know that Hirano bodies contain osmiophilic material, which is consistent with the presence of membrane components. The particulate elements of the array stain with the heavy metal salts uranyl acetate and lead citrate, indicating lipids, nucleo-proteins, and phospholipoproteins (8, 27).

We sought to demonstrate the presence of nucleic acid in the electron-dense particles by staining paraffin sections with the fluorescent dye ethidium bromide, which is specific for nucleic acids by virtue of its ability to intercalate between base pairs (28, 29). The Hirano bodies, identified by concomitant light and fluorescence microscopy of the same specimen at an excitation wavelength of 460 nm, show strong fluorescence with an

emission spectra composed of wavelengths over 590 nm, indicative of nucleic acid. Paraffin sections of hippocampus were then stained at low concentration (0.001%) and pH 3.8 with acridine orange, a fluorescent dye that binds with high affinity to the G·C base pairs of nucleic acids (30, 31), but allows the discrimination of DNA and RNA on the basis of its emission spectra. Once again, the Hirano bodies demonstrated fluorescence with a red component at 656 nm, as expected for RNA. Serving as an internal control, the nuclei of the cells fluoresce yellow-green at 542 nm, characteristic of DNA (32). An example is seen in Fig. 2. We also noted that the Nissl substance of normal pyramidal cells of the hippocampus also binds acridine orange and yields a red fluorescence similar to that of the Hirano body. Virtually no background fluorescence was observed. Control staining was carried out for the presence of acid mucopolysaccharides with colloidal iron and alcian blue at pH 1.5. The results demonstrated that mucopolysaccharides and tissue mucins stained, but Nissl substance, Hirano bodies, and nuclei did not. Thus, the presence of RNA in the electron-dense particles of the Hirano bodies appears to be established and the histological evidence is consistent with a liponucleoprotein structure.

Spatial Filtering. Small sections of electron micrographs of the Hirano bodies such as that shown in Fig. 1*d* were converted to digital arrays at 100-μm intervals along both x and y axes with an Optronics P1000 rotating drum microdensitometer, and the Fourier transform was computed on a PDP 11/40 computer. The area included was 512 by 512 points in size and contained approximately 400 unit cells with about 600 data points per unit cell. The discrete maxima in reciprocal space seen in Fig. 3*A* and listed in Table 1 were used as coefficients in a back Fourier transform by the technique described above. The net effect of this procedure is to filter the micrograph of noise components by ignoring their random contribution to the Fourier transform (i.e., the background) while simultaneously enhancing the periodic elements, and, hence, real elements, of the array that contribute only to the discrete portion of the
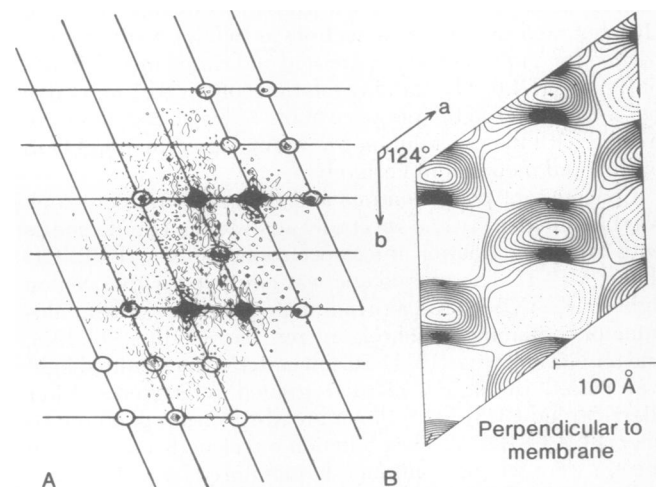

FIG. 3.   Results of digital filtering of the electron micrograph in Fig. 1*d* by Fourier transform methods. (*A*) Fourier transform of the micrograph showing the discrete maxima superimposed on a continuum of random noise. The left and right of the computer-generated transform are contoured at two different levels of intensity to show both the high- and low-resolution maxima. (*B*) The second Fourier transform which includes only the discrete maxima from *A* that fall on the regular reciprocal lattice. The solid-line contours represent density above background level as determined from the statistical analysis of the optical densities over the entire data field. This drawing is the filtered and averaged image of the individual particles that form the arrays on the surfaces on the membranes.

Medical Sciences: O'Brien *et al.*

Proc. Natl. Acad. Sci. USA 77 (1980)   2263

Table 1. Structure factors incorporated in Fourier transform of Hirano bodies

h	k	F	Phase, radians
0	1	58,677	0.700
1	0	8,175	−2.010
0	2	2,006	−0.304
1	3	3,156	−1.100
1	1	55,019	0.180
1	2	4,053	−0.397
2	3	4,023	−1.776
2	4	990	−2.549
2	1	11,259	2.360
2	2	6,094	0.916
3	1	1,386	−1.281
2	1	2,301	0.639
1	2	2,716	−1.925
3	3	1,400	−2.000

transform (i.e., the maxima that fall on a regular lattice). The second result of the procedure is to render an image of the unit cell contents that is essentially the statistically averaged image of the fundamental unit that makes up the array.

The result of the digital filtering and averaging in reciprocal space is shown in Fig. 3B and represents the fundamental asymmetric unit of the Hirano body (i.e., the "electron-dense particle"). The salient feature of this image is its distinctive asymmetrical "skiff" shape, which is very similar to the image of the 60S ribosomal subunit from rat liver obtained by extensive analysis of electron micrographs by entirely different techniques (33–35). This distinctive shape is by all our criteria and tests not artifactual and suggests to us that the electron-dense particle is the large ribosomal subunit rather than the intact ribosome itself. The image we have obtained was reproduced by applying the spatial filtering technique to several different micrographs. In addition, our examination of the tilt-stage photographs tends to confirm the interpretation.

DISCUSSION

Micrographs of Hirano bodies are strikingly similar to those of other observed instances of *in vivo* ribosome crystals (33, 36–41). In particular, the individual strands are almost identical to those seen in the eggs of the lizard *Lacerta sicula* that form during its winter hibernation period (40, 41). Micrographs of these membrane-bound ribosomal arrays appeared on the cover of the September 8, 1977 issue of *Nature* (41) and have been analyzed by Unwin at the MRC Laboratories in Cambridge, England. The arrays are also very similar to those seen in chicken embryos after rapid chilling (33, 37, 38) and those seen in the protozoa *Entamoeba invadens* during its hibernation period (36).

In lizard egg ribosome crystals, the elements appear to be simply collapsed vesicles of endoplasmic reticulum. The sheets are layered face to face, giving rise to clusters of ribosomes sandwiched between membranes. Thus the whole structure is a stack of individual sandwiches. In Hirano bodies, the membrane-ribosome sheets are arranged face to back to form a continuously alternating stack. Whereas the array from the lizard eggs is symmetrical, that from the Hirano bodies is polar.

Lizard egg and chicken embryo ribosomes are arranged into tetramers with P4 symmetry in the planes of the membrane (41, 42). We have not observed this arrangement in Hirano bodies. Instead, sections taken parallel to the sheets that make up the Hirano bodies (confirmed by tilt-stage micrographs ±24° around both a vertical and horizontal axis), like that shown in

Fig. 1d, show that the particles are arranged in a rhombic lattice having cell dimensions $a = b = 130$ Å and $\alpha = 56°$. Each cell contains one particle as the asymmetric unit, with no additional symmetry present.

Our fluorescence microscopy results confirm the presence of RNA and the absence of DNA in the particulate components of the Hirano bodies. In addition, we do not find acid or mucopolysaccharides. The Hirano bodies are osmiophilic but not argentophilic, consistent with the presence of some lipid components (as we might expect from membranes) but inconsistent with neurofilaments. The sizes, shapes, and distribution of the particles along the continuous connecting lines are approximately the same as that of rough endoplasmic reticulum in numerous published examples. The entire array bears a striking resemblance to other observed examples of paracrystalline membrane-ribosomal arrays. In addition, the image of the particles derived from the micrographs by spatial filtering techniques is very similar to that derived for the large eukaryotic ribosome subunit by other investigators using different methods. Thus we believe the cumulative evidence supports the contention that the component "beads on a string" of the Hirano bodies are indeed strips of membrane-bound ribosomes.

It seems to us likely that the membrane-bound ribosomes that comprise the Hirano bodies are derived from the rough endoplasmic reticulum of the normal cell. As we pointed out, the Hirano bodies do stain in a fashion very similar to the Nissl substance, and it is further known that one of the two most prominent effects of neuron damage and trauma is the disappearance of the Nissl substance from the perikaryon around the nuclei (43). The Hirano bodies are generally localized in the same regions of the cell as the endoplasmic reticulum and, as we have pointed out, the distribution of the ribosomes on the membranes seen in the Hirano bodies is the same as that found for the ribosomes on rough endoplasmic reticulum.

That the Hirano bodies are chiefly ribosomes in composition is also consistent with the observations that protein synthesis is decreased in degenerating neural tissue, specifically from patients with presenile and senile dementia. We propose that the neuron, in response to some set of physiological stimuli, has entered a state of reduced protein synthetic activity and retracted its protein-synthesizing mechanisms in a nondestructive fashion. This withdrawal, consolidation, and sequestration of the rough endoplasmic reticulum is manifested by the appearance of the Hirano bodies.

Precedent for this type of phenomenon is found in other occurrences of *in vivo* ribosome crystallization cited previously. All were produced in response to some event signaling or inducing a quiescent state. Indeed, other examples not involving ribosomes are available, as, for example, the storage of apparently defective membrane fragments in vesicles known as zebra bodies in Tay–Sachs and Hurler's storage diseases (44).

The elements of Hirano bodies are not simply collapsed vesicles of endoplasmic reticulum, else they would have the stacking structure of the crystals from the lizard oocytes. They must, in fact, represent a more fragmented state of the Nissl substance because the individual cisternae are not present, but only the component membrane ribosome complexes. Thus we suggest that the Hirano bodies do represent a state of partial endoplasmic reticulum degeneration, but a state that also maintains the essential elements intact.

It is perhaps not coincidental that the Hirano bodies are found predominantly in the hippocampal region of the brain, a region that is associated with the consolidation of short-term to long-term memory (45, 46). One of the more pronounced symptoms of patients with senile dementia is that they retain

long-term memory (i.e., the ability to describe events or sustain skills learned many years previous to the onset of the disease), but they have an impaired capacity to consolidate short-term memory. Thus, it does not appear unreasonable to suggest that the disability of short-term memory could arise because the ribosomes required for synthesis of memory-associated proteins have entered a dormant state and have been stored in a quiescent form resulting in the appearance of the crystalline Hirano bodies.

All of the other known examples of ribosomes crystallizing have occurred in response to some event signaling or inducing a dormant state; e.g., the lizard egg ribosomes that form during hibernation (40, 41) and the ribosomal arrays that occur in the protozoa *Entamoeba invadens* during hibernation (36) and in the chicken embryo after rapid chilling (33, 37, 38). The nature of the signal or the specific condition that induces ribosome storage in the brains of patients with presenile and senile dementia and the possible reversal of the response are questions for further study. However, all of the examples of ribosomal storage cited above are reversible, and this could be true of those found in human brain as well.

1. Hirano, A., Malamud, N., Elizan, T. S. & Kurland, L. T. (1966) *Arch. Neurol.* **15,** 35–41.
2. Schochet, S. S., Jr., Hardman, J. M., Ladewig, P. P. & Earle, K. M. (1969) *Arch. Neurol.* **20,** 548–553.
3. Field, E. J., Mathews, J. D. & Raine, C. S. (1969) *J. Neurol. Sci.* **8,** 209–224.
4. David-Ferreira, J. F., David-Ferreira, K. L., Gibbs, C. J. & Morris, J. (1968) *Proc. Soc. Exp. Biol. Med.* **127,** 313–320.
5. Anzil, A. P., Herrlinger, H., Blinzinger, K. & Heldrick, A. (1974) *Arch. Neurol.* **31,** 94–100.
6. Hirano, A. & Dembitzer, H. M. (1976) *Neurobiology* **2,** 225–232.
7. Powers, J. M., Balentine, J. D., Wisniewski, H. M. & Terry, R. D. (1976) *J. Neuropathol. Exp. Neurol.* **35,** 14–25.
8. Schochet, S. S. & McCormick, W. F. (1972) *Acta Neuropathol.* **21,** 50–60.
9. Tomonaga, M. (1974) *Acta Neuropathol.* **28,** 365–366.
10. Hirano, A., Dembitzer, H. M., Kurland, L. T. & Zimmerman, H. M. (1968) *J. Neuropathol. Exp. Neurol.* **27,** 167–182.
11. Thompson, S. W. (1966) *Selected Histochemical and Histopathological Methods* (Thomas, Springfield, IL).
12. Ogata, J., Budgilovich, G. N. & Cravioto, H. (1972) *Acta Neuropathol.* **21,** 61–67.
13. LePecq, J. B. (1971) *Methods Biochem. Anal.* **20,** 41–86.
14. Combs, J. (1973) *Microscope* **21,** 11–21.
15. Klug, A. & Berger, J. E. (1964) *J. Mol. Biol.* **10,** 565.
16. Erickson, H. P. & Klug, A. (1971) *Phil. Trans. R. Soc.* **261B,** 105–118.
17. Brigham, E. O. (1974) *The Fast Fourier Transform* (Prentice-Hall, Englewood Cliffs, NJ), pp. 91–95.
18. Castleman, K. R. (1979) *Digital Image Processing* (Prentice-Hall, Englewood Cliffs, NJ).
19. Saxton, W. O. (1978) *Computer Techniques for Image Processing in Electron Microscopy,* Suppl. 10 (Academic, New York), p. 196.
20. Gonzalez, R. C. & Wintz, P. (1977) *Digital Image Processing* (Addison-Wesley, London), pp. 50–51.
21. Abei, U., Smith, P. R., Dubochet, J., Henry, C. & Kellenberger, E. (1973) *J. Supramol. Struct.* **1,** 498–522.
22. Cooley, J. W. & Tukey, J. W. (1965) *Mass Computation* **19,** 297–301.
23. Fraser, R. D. B. & Millward, G. R. (1970) *J. Ultrastruct. Res.* **31,** 203–211.
24. Van Holde, K. E. & Hill, W. E. (1974) in *Ribosomes,* eds. Nomura, S., Tissieres, X. & Lengyel, P. (Cold Spring Harbor Laboratory, Cold Spring Harbor, NY), pp. 53–91.
25. Palade, G. E. (1955) *J. Biophys. Biochem. Cytol.* **1,** 59–68.
26. Palade, G. E. & Siekevitz, P. (1956) *J. Biophys. Biochem. Cytol.* **2,** 171–200.
27. Towfighi, J. (1972) *Acta Neuropathol.* **21,** 224–231.
28. Crissman, H. A., Oka, M. S. & Steinkamp, J. A. (1976) *J. Histochem. Cytochem.* **24,** 64–71.
29. Mackie, C., Bryant, T. H. E. & Mowbray, J. (1978) *Biochem. J.* **177,** 977–979.
30. Rigler, R. (1966) *Acta Physiol. Scand.* **67,** 7–11.
31. Schümmelfeder, N. (1958) *J. Histochem. Cytochem.* **6,** 392–393.
32. West, S. & Lorinez, A. (1973) in *Fluorescence Techniques in Cell Biology,* eds. Thaer, A. A. & Sernetz, M. (Springer, New York), pp. 395–407.
33. Lake, J. A., Sabatini, D. D. & Nonomura, Y. (1974) in *Ribosomes,* eds. Nomura, S., Tissieres, X. & Lengyel, P. (Cold Spring Harbor Laboratory, Cold Spring Harbor, NY), pp. 543–557.
34. Brimacombe, R., Staffler, G. & Wittman, H. G. (1978) *Annu. Rev. Biochem.* **47,** 217–249.
35. Cox, R. A. (1977) *Prog. Biophys. Mol. Biol.* **32,** 193–231.
36. Lake, J. A. & Slayter, H. S. (1971) *J. Mol. Biol.* **66,** 271–278.
37. Byers, B. (1966) *J. Cell Biol.* **30,** C1–C6.
38. Byers, B. (1967) *J. Mol. Biol.* **26,** 155–167.
39. Carey, N. H. & Read, G. S. (1971) *Biochem. J.* **121,** 511–519.
40. Taddei, C. (1972) *Exp. Cell Res.* **70,** 285–292.
41. Unwin, P. N. T. (1977) *Nature (London)* **269,** 118–122.
42. Unwin, P. N. T. & Taddei, C. (1977) *J. Mol. Biol.* **114,** 491–506.
43. Cajal, S. R. Y. (1968) *Degeneration and Regeneration of the Nervous System* (Hofner, London), pp. 521–523.
44. Escourolle, R. & Poirier, J. (1978) *Manual of Basic Neuropathology* (Saunders, Philadelphia).
45. Green, J. D. (1964) *Physiol. Rev.* **44,** 561–608.
46. Drachman, D. A. & Arbit, J. (1966) *Arch. Neurol.* **15,** 52–61.